

## Article

# Local Track Irregularity Identification Based on Multi-Sensor Time–Frequency Features of High-Speed Railway Bridge Accelerations

Ye Mo <sup>1</sup>, Yi Zhuo <sup>2</sup> and Shunlong Li <sup>1,\*</sup> 

<sup>1</sup> School of Transportation Science and Engineering, Harbin Institute of Technology, 73 Huanghe Road, Harbin 150090, China

<sup>2</sup> China Railway Design Corporation, Tianjin 300142, China

\* Correspondence: lishunlong@hit.edu.cn; Tel.: +86-0451-86283779

**Abstract:** Shortwave track diseases are generally reflected in the form of local track irregularity. Such diseases will greatly impact the train–track–bridge interaction (TTBI) dynamic system, seriously affecting train safety. Therefore, a method is proposed to detect and localize local track irregularities based on the multi-sensor time–frequency features of high-speed railway bridge accelerations. Continuous wavelet transform (CWT) was used to analyze the multi-sensor accelerations of railway bridges. Moreover, time–frequency features based on the sum of wavelet coefficients were proposed, considering the influence of the distance from the measurement points to the local irregularity on the recognition accuracy. Then, the multi-domain features were utilized to recognize deteriorated railway locations. A simply-supported high-speed railway bridge traversed by a railway train was adopted as a numerical simulation. Comparative studies were conducted to investigate the influence of vehicle speeds and the location of local track irregularity on the algorithm. Numerical simulation results show that the proposed algorithm can detect and locate local track irregularity accurately and is robust to vehicle speeds.

**Keywords:** local track irregularity identification; high-speed railway bridge; TTBI dynamic system; CWT; multi-sensor time–frequency features



**Citation:** Mo, Y.; Zhuo, Y.; Li, S. Local Track Irregularity Identification Based on Multi-Sensor Time–Frequency Features of High-Speed Railway Bridge Accelerations. *Sustainability* **2023**, *15*, 8237. <https://doi.org/10.3390/su15108237>

Academic Editor: Pablo Rodríguez-González

Received: 6 March 2023

Revised: 9 May 2023

Accepted: 15 May 2023

Published: 18 May 2023



**Copyright:** © 2023 by the authors. Licensee MDPI, Basel, Switzerland. This article is an open access article distributed under the terms and conditions of the Creative Commons Attribution (CC BY) license (<https://creativecommons.org/licenses/by/4.0/>).

## 1. Introduction

In the straight section of track lines, the difference in geometric parameters produced by the rail relative to the standard straight track position is called track irregularity [1]. During the operation of high-speed railroads, track irregularities are the primary cause of abnormal train vibration. With the increased train running speed, even a small amplitude of track irregularity may cause strong vibration between wheels and rails. Consequently, track quality assessment has become a hot issue in transportation safety research. It is critical for developing damage detection methods that minimize disruptions to the transportation network.

Nowadays, high-speed lines mainly use ballastless tracks so the rail mainly has shortwave diseases. Moreover, shortwave track diseases are generally manifested as local track irregularities. Garg and Dukkipati [2] describe the various typically local irregularity expressions reported in field measurements. Such irregularity will cause an additional impact force from the wheel–rail force and accelerate the deterioration of the rail. Worse, the additional impact force will be transmitted to the under-rail bridge structure through the bridge–rail interaction point, causing potential damage to the bridge structure. Therefore, shortwave track diseases must be detected and maintained as early as possible.

Regularly detecting the health status of the railway system through the track inspection car is the main traditional method [3–5]. However, this method is inefficient and cannot accurately reflect the dynamic track irregularity under the actual train operation.

Researchers found that train vibration responses contain information on track conditions and disease. Kouroussis et al. [6] analyzed the vibration impact on the ground due to vehicle excitation caused by local irregularity on the track. This analysis found that the vibration energy is significantly higher when there is local damage. Therefore, it is of practical significance to study track irregularity based on train vibration response.

The measurement of axle-box acceleration (ABA) signals does not require complex instrumentation and the accelerometers can be easily fixed outside the axle box. In recent years, many research teams at home and abroad have identified track operation status by monitoring ABA signals [7–12]. The technology is easy to implement, low cost, and has the potential for real-time monitoring. For example, Li et al. [13,14] proposed a finite element model-based algorithm for the early monitoring of track depressions. They pointed out that ABA is sensitive to short-wave irregularity. Molodova et al. [15] indicated that the peak of ABA and its local frequency characteristics may be quantitatively related to the size of the defect. Lin et al. [8] used EMD (empirical mode decomposition) and Cohen's class distribution algorithms to analyze ABA and the proposed algorithm can be applied to track irregularity measurements. Yuan et al. [16] used the CVAE (conditional variational auto encoder)-elliptic envelope method to detect and identify the rail squats. Zhang et al. [17] proposed an algorithm to localize tunnel damage using ABA signals and WPE (wavelet packet energy)-CVAE.

The bridge structure health monitoring system (BSHM) is equipped with many sensors at different positions of the bridge structure to monitor the operation status of the bridge [18–20]. Over the past decades, many scholars have conducted in-depth studies on various types of monitoring data in BSHM systems. For example, Bao et al. [21] used sparse time–frequency analysis of cable force acceleration to identify time-varying cable tension. Huang et al. [22] developed a method based on Gibbs sampling to solve the problem of sparse stiffness identification. Li et al. [23] modeled the cable tension ratio model using a Gaussian mixture model to evaluate the state of the diagonal cable.

The BSHM monitoring data contains a wealth of structural state information. When there is a local irregularity in the track structure, the additional local excitation will be transmitted to the bridge structure through the track–bridge interaction point, affecting the train-induced bridge accelerations. Therefore, this study analyzes train-induced bridge accelerations at different measuring points to identify the local track irregularity.

The proposed algorithm aims to identify and locate the track structure's local irregularity. Continuous wavelet transform (CWT) extracts train-induced bridge response features. In the train–track–bridge interaction (TTBI) system, the existence of local track irregularity is equivalent to the additional external excitation imposed on the bridge. Thus, additional energy is generated in the train-induced bridge responses. Moreover, the sum of wavelet coefficients over the full scale can reflect the energy distribution of responses in the time domain. Consequently, this paper uses the sum of wavelet coefficients over the full scale to identify local track irregularities. The local peaks of the sum of wavelet coefficients can reflect the location information of local track irregularities in the spatial domain. This paper uses the local peaks of the sum of wavelet coefficients as the localization indicator.

The remaining paper is organized as follows. Section 2 illustrates the proposed methodology and briefly introduces the excitation of local track irregularity in TTBI system vibration. A numerical verification through TTBI simulation is demonstrated in Section 3. Section 4 draws the main conclusions.

## 2. Theoretical Background

### 2.1. Excitation of Local Track Irregularity in TTBI System Vibration

With increasing rail capacity and speed, the problem of train–track–bridge interaction (TTBI) has become more prominent. The theory of TTBI dynamics has opened up a new field of railroad system dynamics research, creatively studying relatively independent subsystems as a large unified system [24–27].

The presence of track irregularities changes the wheel–rail contact relationship and impacts the dynamic characteristics of the wheel–rail system. The vehicles vibrate under the excitation of track irregularities and other external excitations. Moreover, the vibration is then transferred to the track and bridge through the wheel–rail contact points, thus forming the dynamic interaction process of the TTBI system [24]. Therefore, track irregularity is considered one of the main sources of self-excited excitation for the TTBI system vibration. Its frequency domain characteristics will significantly affect the dynamic response of bridges and vehicles. The frequency domain characteristics embody the overall fluctuation state of track irregularity. In this section, the harmonic irregularity curve of a single frequency component is selected as the analysis sample:

$$w(x) = \frac{A}{2} \left( 1 - \cos \frac{2\pi x}{l} \right) \quad x \in [a, b] \quad (1)$$

in which,  $A$  and  $l$  are the amplitude and wavelength of irregularity, respectively;  $x$  is the position of irregularity; and interval  $[a, b]$  is the position range of irregularity.

Based on the wheel–track corresponding assumption, the vertical displacement of the wheel  $z(t)$  can be expressed as:

$$z(t) = y(x, t) + w(x) \quad (2)$$

where  $y(x, t)$  and  $w(x)$  are the vertical vibration displacement of the bridge and the displacement caused by track irregularity, respectively.

The vertical force on the simply-supported beam could be simplified as follows:

$$P(x, t) = M_1 g - M_1 \frac{d^2 z(t)}{dt^2} \quad (3)$$

in which  $\frac{d^2 z(t)}{dt^2} \approx \frac{\partial^2 y(x, t)}{\partial t^2} + \frac{\partial^2 w(x)}{\partial t^2}$ ;  $M_1$  is the mass of moving load; and  $g$  is gravity acceleration.

In summary, the additional local force  $P_{\cos}(t)$  generated by harmonic irregularity can be expressed as:

$$P_{\cos}(t) = M_1 \frac{\partial^2 w(x)}{\partial t^2} = \frac{2\pi^2 v^2 M_1 A}{l^2} \cos \frac{2\pi vt}{l} = P \sin \bar{\omega} t \quad t \in \left[ \frac{a}{v}, \frac{b}{v} \right] \quad (4)$$

where  $P = \frac{2\pi^2 v^2 M_1 A}{l^2}$ ,  $\bar{\omega} = \frac{2\pi vt}{l} + \frac{\pi}{2}$ . Equation (4) shows that the effect of local harmonic irregularity on the beam structure can be equivalent to a moving harmonic load.

From the Duhamel integral [28], generalized coordinates of the  $n$ -th mode of the supported beam under the action of  $P_{\cos}(t)$  are written as:

$$q_n(t) = \frac{2}{mL\omega_D^n} \int_{a/v}^{b/v} P \sin \bar{\omega} \tau \sin n\omega \tau e^{-\omega_b(t-\tau)} \sin \omega_D^n(t-\tau) d\tau \quad (5)$$

where  $q_n(t)$  is the generalized coordinates of the  $n$ -th mode;  $\omega_b = \xi_n \omega_n$  is critical damping frequency; and  $\omega_D^n$  is the  $n$ -th damped natural frequency.

According to the trigonometric transformation formula [29], Equation (5) can be further written as:

$$q_n(t) = \frac{P}{mL} \left\{ \frac{(\omega_n^2 - r_2^2) - (\cos r_2 t - A) + 2\omega_b r_2 \sin r_2 t - \frac{\omega_b}{\omega_D^n} (\omega_n^2 + r_2^2) A}{(\omega_n^2 - r_2^2)^2 + 4\omega_b^2 r_2^2} - \frac{(\omega_n^2 - r_1^2) - (\cos r_1 t - A) + 2\omega_b r_1 \sin r_1 t - \frac{\omega_b}{\omega_D^n} (\omega_n^2 + r_1^2) A}{(\omega_n^2 - r_1^2)^2 + 4\omega_b^2 r_1^2} \right\} \quad (6)$$

where  $r_1 = \bar{\omega} + n\omega$ ,  $r_2 = \bar{\omega} - n\omega$ ,  $\omega = \pi v/L$  and  $A = e^{-\omega_b t} \sin \omega_D^n t$ .

Thus, the acceleration of the bridge under the action of local harmonic irregularity can be expressed as:

$$\ddot{y}_{\cos}(x, t) = \sum_{n=1}^{\infty} \ddot{q}_n(t) \sin \frac{n\pi x}{L} \quad (7)$$

From Equation (7), it can be seen that under the action of moving harmonic force, the mid-span acceleration of the simply-supported beam under the action of moving harmonic force can be regarded as the superposition of three harmonic curves. That is, one frequency is  $\omega_D^n$ , and the other two frequencies are  $r_1$  and  $r_2$ , respectively. It is shown that when there are local harmonic irregularities in the track structure, the high-speed operation of the train leads to additional medium- and high-frequency components in bridge accelerations. These frequency components are related to the train speed and the wavelength of the local harmonic irregularities.

## 2.2. Time–Frequency Features Extraction

Continuous wavelet transform (CWT) performs multi-scale signal refinement by scaling translation operation, which has high resolution and adaptability. For the bridge acceleration signal  $x(t)$ , its CWT form can be expressed as [28]:

$$W_x(a, t) = x(t) \times \psi_a(t) = x(t) \times \left( a \frac{d\theta_a(t)}{dt} \right) = a \frac{d}{dt} [x(t) \times \theta_a(t)] \quad (8)$$

where  $a$  is the scale parameter, the wavelet function  $\psi(t) = \frac{d\theta(t)}{dt}$ ,  $\theta(t)$  is a smooth function and satisfies  $\int_{-\infty}^{\infty} \theta(t) dt = 1$  and it is a higher order infinitesimal of  $\frac{1}{1+t^2}$ ;  $\theta_a(t) = a \times \theta(\frac{t}{a})$  is the original wavelet function.

The absolute value of the sum of wavelet coefficients on the whole scale can be expressed as:

$$S(b) = \sum_{j=1}^n |W_x(a, t)| \quad (9)$$

in which  $n$  is the number of scales.

The inflection points of  $W_x(a, t)$  occur when the signal  $x(t)$  changes abruptly. At this time,  $S(b)$  has a maximum value. Therefore, the mutation point of the signal can be found when the wavelet coefficient is maximized. From the derivation of Section 2.1, it can be seen that local track irregularity is equivalent to the additional harmonic force applied to the simply-supported beam. When the train passes through the local irregularity, the dynamic response of the bridge will have different degrees of mutation here. Therefore, by analyzing the bridge accelerations and then performing CWT, the local irregularity can be detected and located by analyzing the sum of wavelet coefficients  $S(b)$ .

## 2.3. Local Track Irregularity Identification Based on Multi-Sensor Time–Frequency Features

In previous sections, it was shown that the sum of wavelet coefficients effectively identifies the additional effects caused by local unevenness on the train-induced bridge responses. Moreover, the local peaks of the sum of wavelet coefficients reflect the potential location information of local track irregularities.

The detection process can be divided into the following steps:

Step 1: CWT is performed on the acceleration of multiple measuring points, and the sum of wavelet coefficients  $S_i(b)$  is extracted as the identification index-1. Among them, index-1 is used to detect whether there is local track irregularity.

Step 2: The corresponding threshold  $F_i$  is defined for different measuring points based on the baseline case. When the index-1 of a measuring point  $i$  exceeds  $F_i$ , it is considered that there is local track irregularity.

Step 3: The degree of abrupt variation between multiple measurement points is compared to determine which ones are far from the local irregularity. The data from these measurement points are excluded from the subsequent positioning analysis.

The location of local peaks of index-1 is further extracted for localization, which is recorded as index-2. For trains with multiple cars, their wheels repeatedly pass through local irregularity, which makes index-2 exhibit periodicity in space. The periodicity interval is closely related to the spatial distribution of wheels. When the extracted local peak position conforms to the spatial distribution of the wheel at the spatial interval, the location of the local irregularity can be identified. The flow chart of the algorithm in this paper is shown in Figure 1.

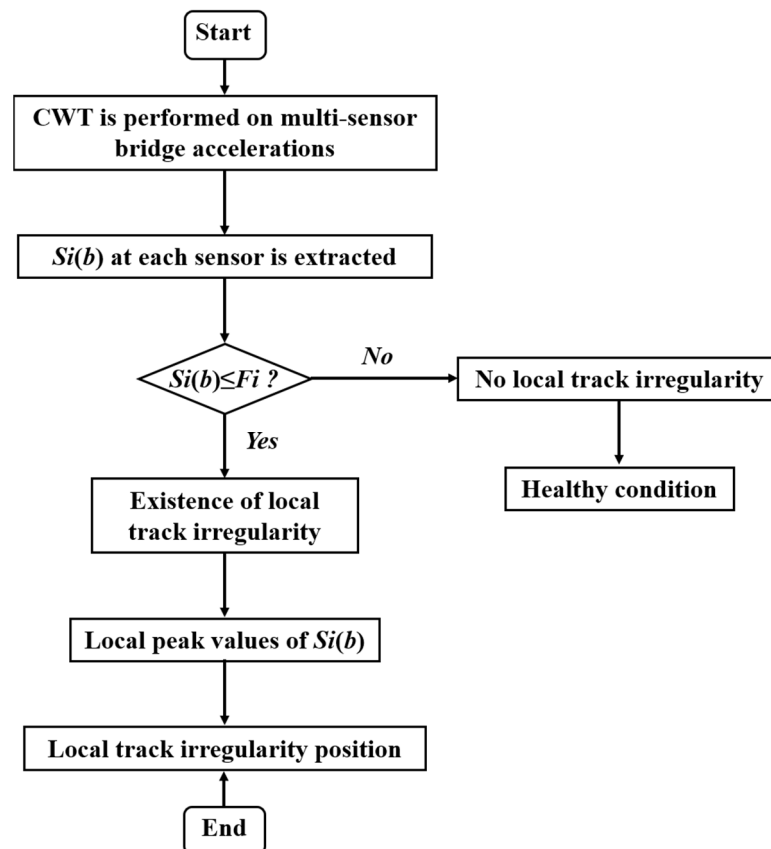
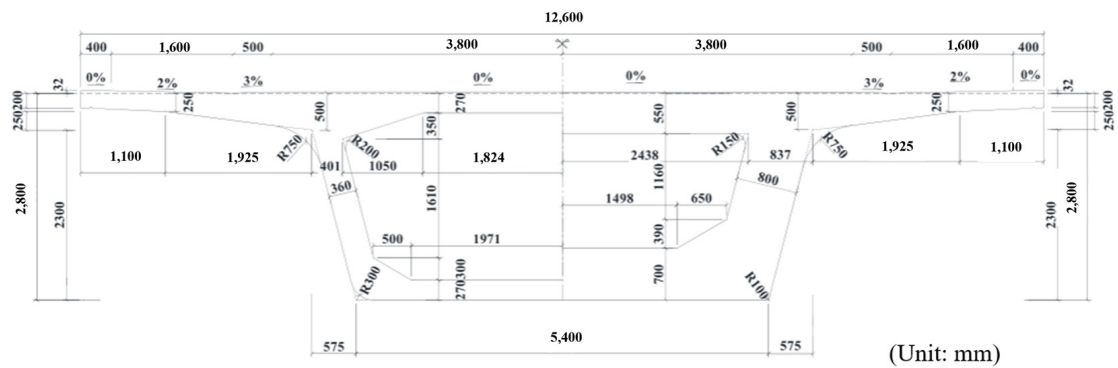


Figure 1. The flow chart of the proposed algorithm.

### 3. Numerical Simulation

#### 3.1. The Finite Element Model of High-Speed Railway Bridge

In this section, numerical analysis was performed using the universal mechanism (UM) dynamics model of a high-speed railway simple-supported bridge. The simply-supported beam bridge adopted the single-box single-compartment section. The total length of the bridge was 32.6 m, and its cross-section is shown in Figure 2 [30]. The simulation analyzed the vertical acceleration at the five measuring points on the center line of the box girder floor, including the three points where the three sections of the bridge  $L/4$ ,  $L/2$ , and  $3L/4$  intersect with the center line of the box girder floor, and the two points on the center line of the box girder floor adjacent to both ends of the beam. The sampling frequency  $f_s$  was taken as 500 Hz.



**Figure 2.** The cross-section diagram of the box girder.

The vehicle was a three-dimensional space model, using the CRH380A EMU train, which consists of two motor cars and six trailers. The parameters modeling of the actual train were referenced and the model was modeled concerning the parameters of the actual train.

Moreover, the continuous elastic foundation beam model was selected as the track model in the U.M. program. The rail model can be approximated as a continuous elastic beam. The rail was connected to the under-rail foundation as a parallel connection of a linear spring and damper system while laterally viewed as a series combination. Furthermore, the CN60 rail used for the rails was the Chinese standard 60 kg/m rail. Figure 3 shows the dynamic model of the TTBI system.

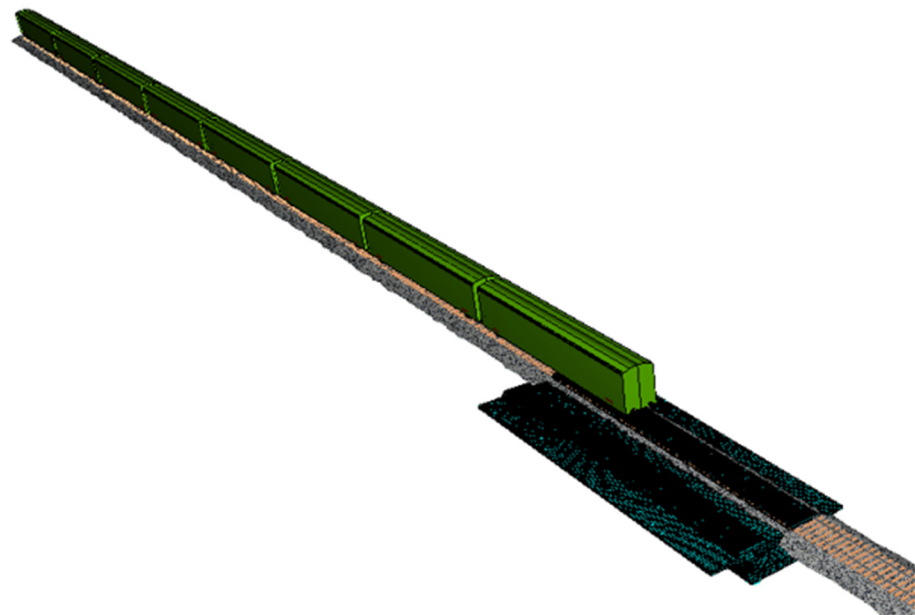


**Figure 3.** Multi-body dynamics model diagram of the TTBI system.

### 3.2. Local Track Irregularity Simulation

In this section, the amplitude of local harmonic irregularity was set to 1 mm; the wavelength was 500 mm. Moreover, the local irregularity position was set as 8 m, 16 m, and 24 m, respectively, denoted as single-1, single-2, and single-3 cases. To further investigate the applicability of the proposed method to multi-point local irregularity identification, multiple-1, multiple-2, and multiple-3 cases were defined. They were located at 8 m + 16 m,

8 m + 24 m, and 16 m + 24 m, respectively. The damaged track irregularity is the sum of initial random and local irregularities, as shown in Equation (10).

$$w_r(x) = w_i(x) + w_s(x) \quad (10)$$

in which,  $w_r$ ,  $w_i$ , and  $w_s$  are the damaged track irregularity, initial random track irregularity, and local irregularity, respectively. The CRH2018 track irregularity spectrum is adopted in this simulation as the initialized random track irregularity. Figure 4 exhibits the generated damaged track irregularity of single-1 case.

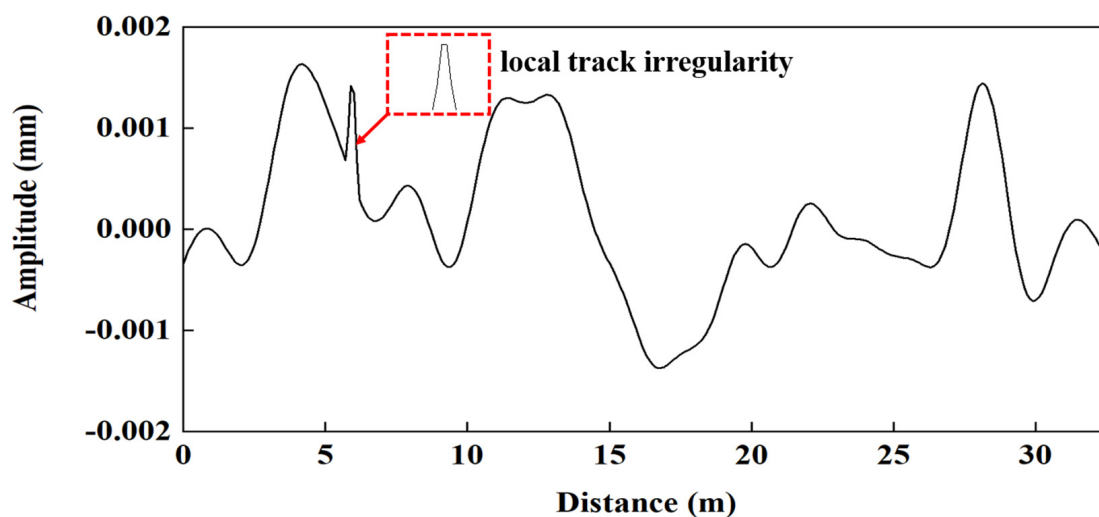


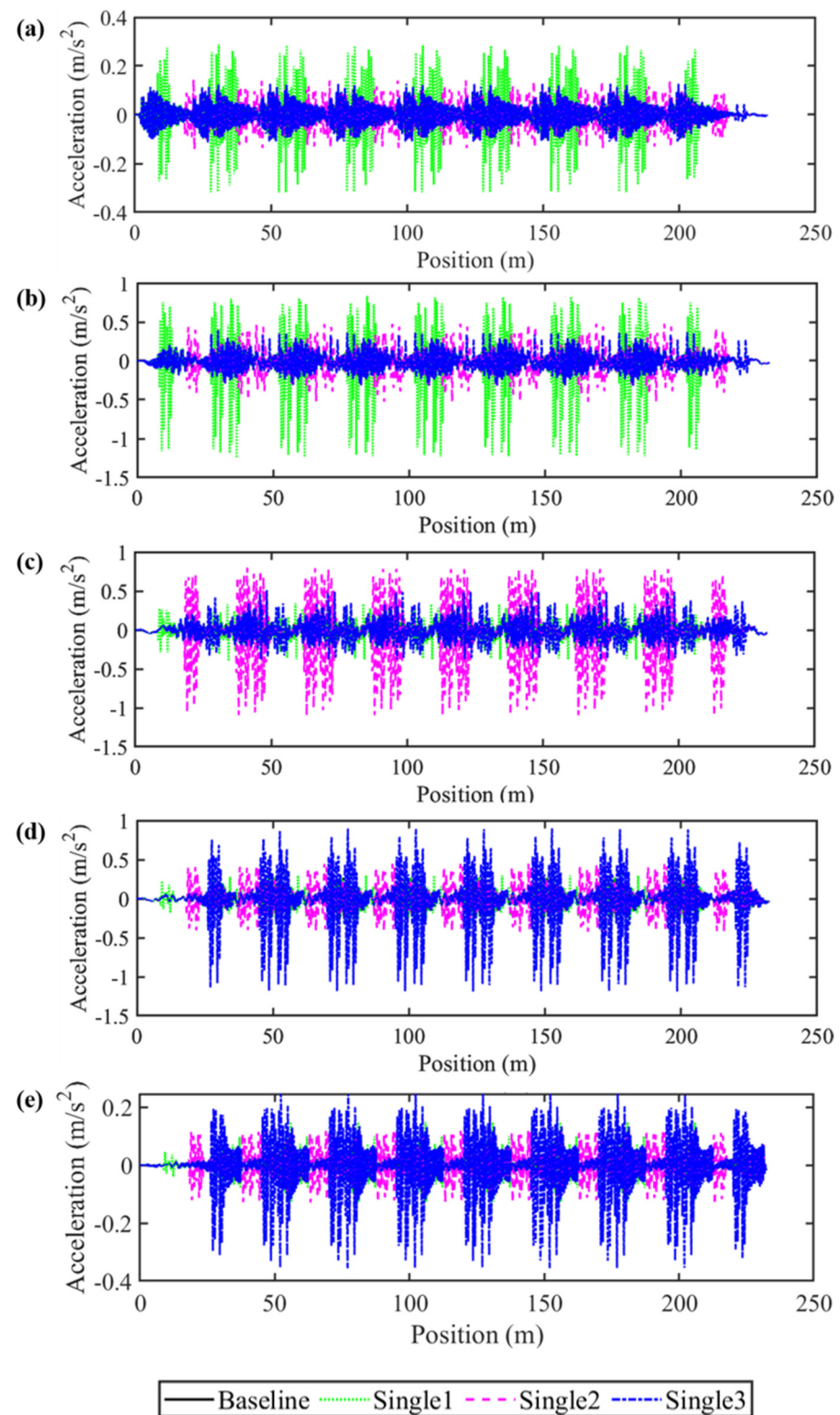
Figure 4. Accumulated track irregularity of single 1.

#### 4. Discussion of Research Results

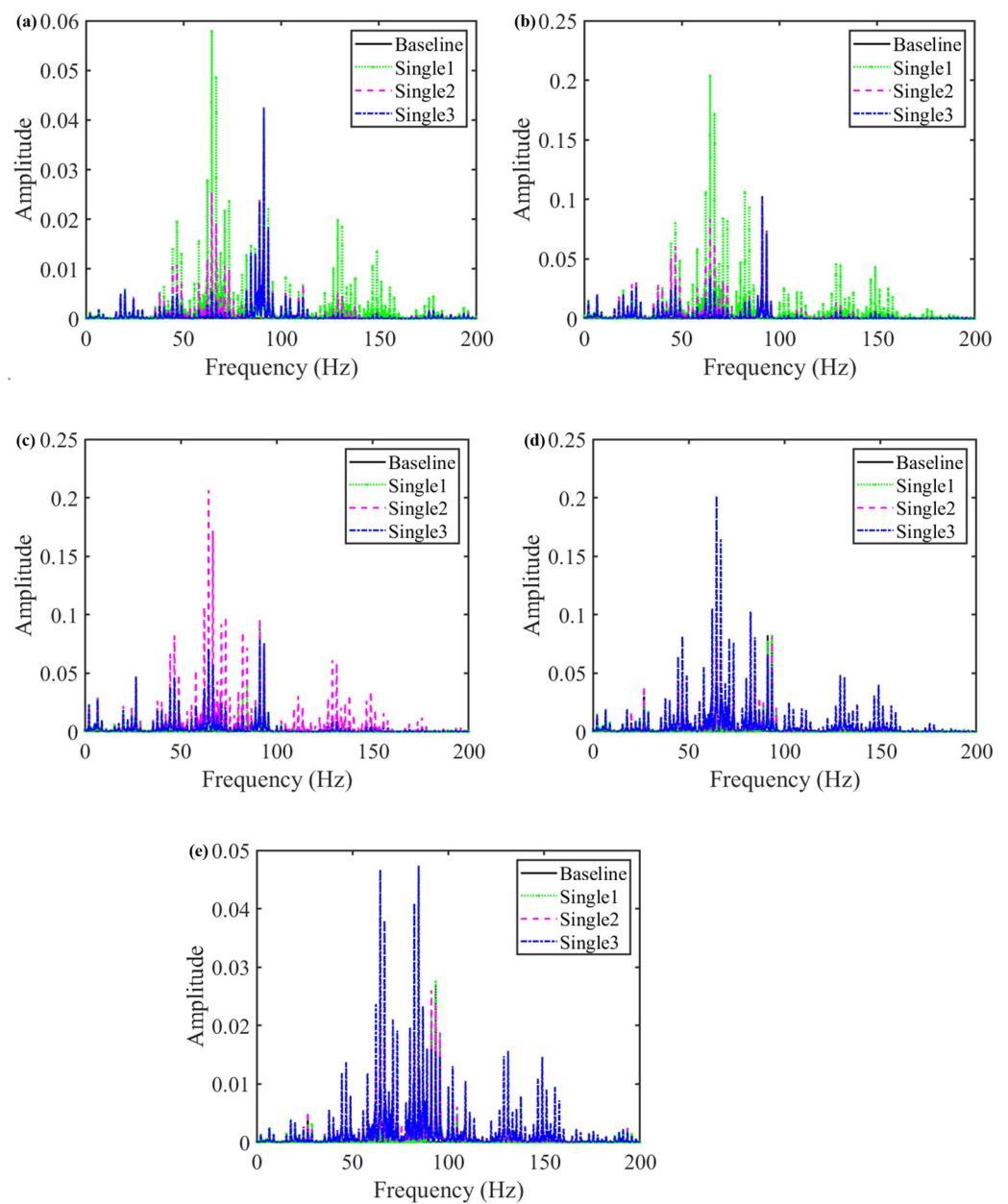
##### 4.1. Multi-Domain Characteristics of Bridge Acceleration

Figure 5a–e show the bridge accelerations at the five measurement points. It can be seen that a single local harmonic irregularity causes a sudden change in bridge acceleration in the spatial domain when the vehicle passes through the local harmonic irregularity. Due to the repeated action of multiple trains, the sudden change exhibits an obvious periodicity in the spatial domain. The spatial intervals are related to the spatial distribution of the cars (about the length of a single carriage). The farther the measurement point is from the local unevenness, the less its measured bridge acceleration differs from the baseline model in the spatial domain. Figure 5 suggests that the bridge acceleration response using multiple measurement points can better capture the abrupt changes in acceleration response caused by harmonic irregularities at different locations.

Figure 6a–e show the frequency domain characteristics of bridge acceleration at different measurement points. It can be concluded that the local harmonic irregularities cause medium- and high-frequency vibrations. However, it consists of multiple high dominant frequencies, which indicates that the bridge acceleration caused by local harmonic irregularities is not a single impulse signal. The frequency domain characteristics of bridge acceleration at different measuring points also differ in sensitivity to local harmonic irregularity. When the measuring point is closer to the local harmonic irregularity, it is easier to capture the influence of local harmonics on bridge acceleration.



**Figure 5.** Vertical bridge acceleration in the spatial domain at five measurement points: (a) measurement point 1; (b) measurement point 2; (c) measurement point 3; (d) measurement point 4; (e) measurement point 5.



**Figure 6.** Vertical bridge acceleration in the frequency domain at five measurement points: (a) measurement point 1; (b) measurement point 2; (c) measurement point 3; (d) measurement point 4; (e) measurement point 5.

Since the frequency domain characteristics lose the time-varying characteristics of the acceleration response, further study of the time–frequency characteristics of multi-sensor bridge acceleration is necessary. Figure 7 is the acceleration wavelet time–frequency diagram at different measuring points. From the diagram, it can be seen that under the excitation of the baseline random track irregularity, there are nine energy concentration areas at measuring points 2–4, which are closely related to the spatial position of the wheelset. As measuring points 1 and 5 are near the end of the bridge, there are 16 energy concentration areas. Under the excitation of train load and random track irregularity, the acceleration response of the bridge will produce high-frequency vibration, mainly concentrated at 60–130 Hz.

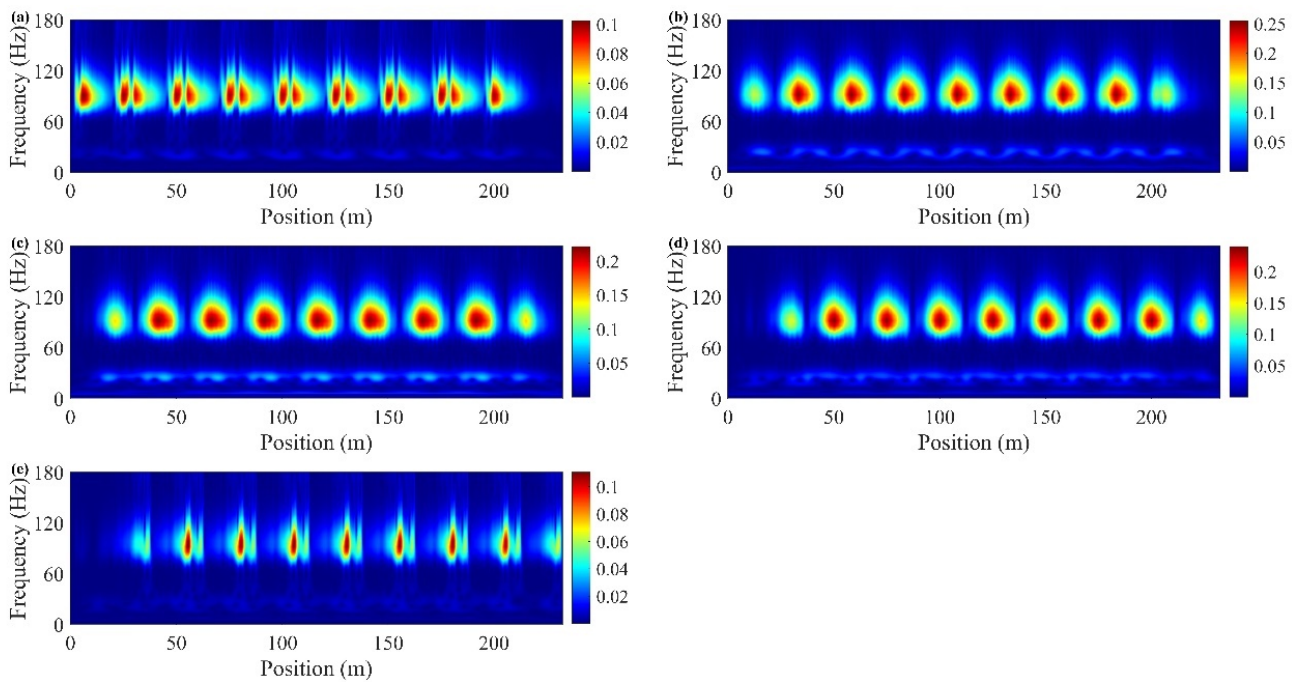


**Figure 7.** Time–frequency diagram of bridge acceleration under baseline case: (a) measurement point 1; (b) measurement point 2; (c) measurement point 3; (d) measurement point 4; (e) measurement point 5.

Figure 8 is the wavelet time–frequency diagram of bridge acceleration when a local harmonic irregularity is at 8 m. It can be implied from Figure 8 that due to local harmonic irregularity, the wavelet time–frequency energy has a significant mutation. The energy mutation generated by measuring points 1 and 2 near 8 m is the most obvious. The first position of the mutation is about 8–10 m, and the mutation position is spatially periodic.

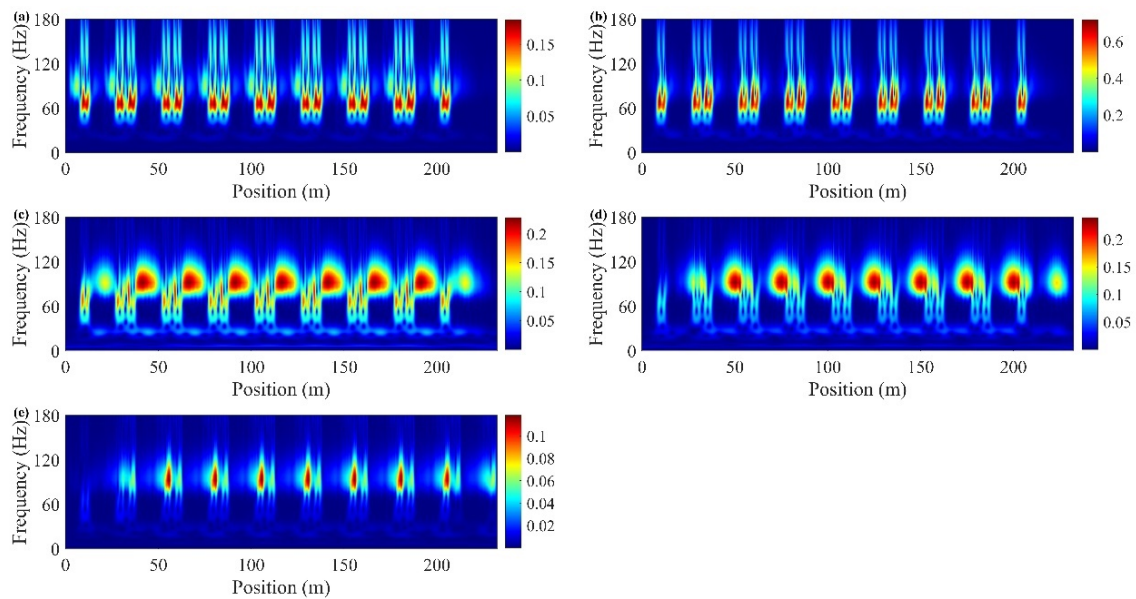


**Figure 8.** Time–frequency diagram of bridge acceleration under Single-1 case: (a) measurement point 1; (b) measurement point 2; (c) measurement point 3; (d) measurement point 4; (e) measurement point 5.

In summary, the time–frequency domain can capture the additional response caused by local harmonic irregularity. Therefore, this paper uses the sum of wavelet coefficients at full scale for further analysis.

#### 4.2. Data Generation and Feature Extraction

The established TTBI dynamic model is used to generate data for algorithm verification. In order to investigate the effect of vehicle speed on the proposed algorithm, 100 vehicle speed samples were generated within the interval [200,250] km/h and subjected to a uniform distribution. It can be summarized in the following steps:

Step 1: Track irregularity generation by Equation (10) and input to the TTBI dynamic model.

Step 2: Calculation of vertical bridge acceleration at multiple measuring points.

Step 3: Extraction of the sum of wavelet coefficients of the calculated accelerations.

In this section, the acceleration during the train crossing the bridge is chosen for analysis. The different train speeds make the calculated acceleration samples unequal in length. Thus, spatial domain resampling obtains the spatial-domain acceleration with equal spatial intervals.

#### 4.3. Local Track Irregularity Detection

In this simulation, threshold  $F_i = \mu_i + 3\sigma_i$ ,  $\mu_i$  and  $\sigma_i$  are the mean and standard deviation of index-1 extracted from the baseline case, respectively. Figure 9 shows the sum of wavelet coefficients at full scale for the four conditions at a vehicle speed of 200 km/h. The figure shows that the sum of wavelet coefficients of bridge acceleration at each measurement point is much smaller in the baseline condition compared with the local irregularity condition. The sum of wavelet coefficients has a larger peak when the measurement point is closer to the local irregularity. When the measurement point is far from the local irregularity, the peak of the sudden change is smaller, and it is challenging to distinguish whether there is local track irregularity.

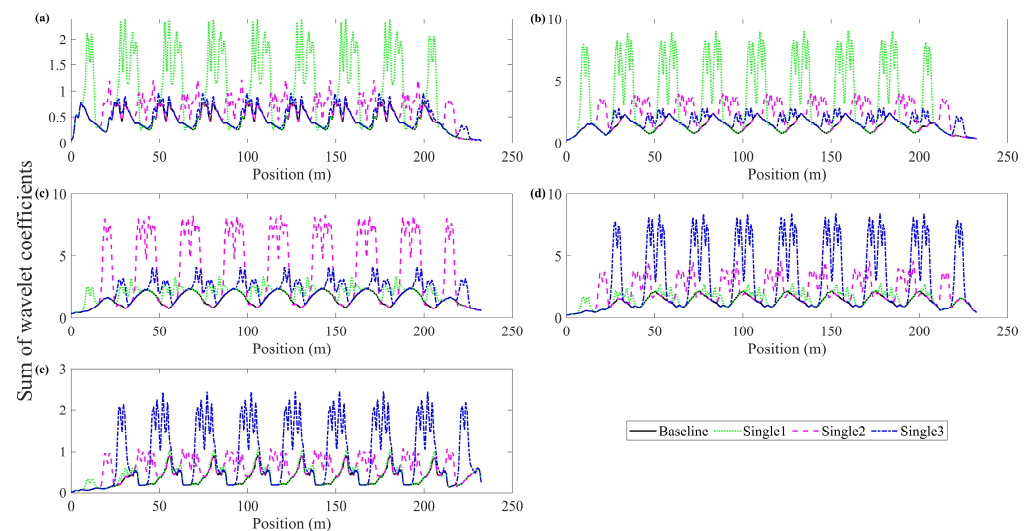


**Figure 9.** Sum of wavelet coefficients at vehicle speed 200 km/h: (a) measurement point 1; (b) measurement point 2; (c) measurement point 3; (d) measurement point 4; (e) measurement point 5.

The time–frequency characteristics of bridge acceleration at 250 km/h are further analyzed, as shown in Figure 10. Comparing Figures 9 and 10 show that speed has little influence on the results of the proposed index-1. Local track irregularity can be detected by comparing the multi-sensor index-1 values in the baseline condition with other operating conditions. Figure 11 shows the sum of wavelet coefficients at 100 train speeds, which obey a random distribution in the interval of (200, 250) km/h.

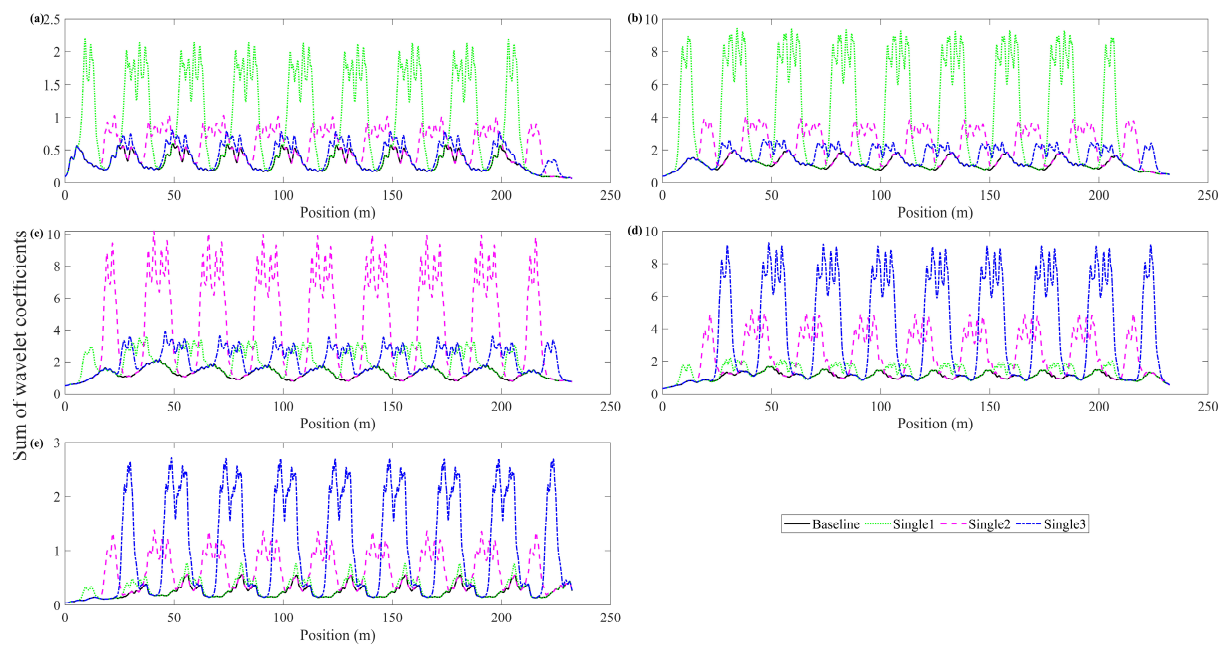


**Figure 10.** Sum of wavelet coefficients at vehicle speed 250 km/h: (a) measurement point 1; (b) measurement point 2; (c) measurement point 3; (d) measurement point 4; (e) measurement point 5.

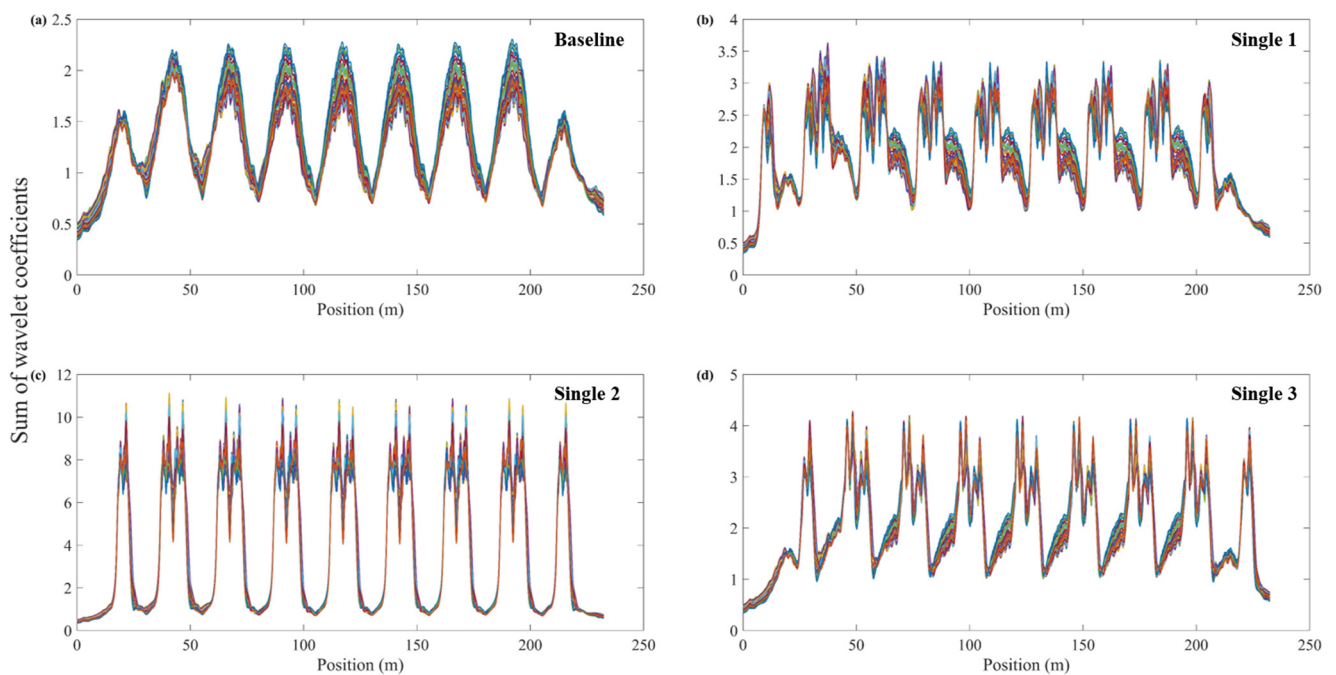


**Figure 11.** Sum of wavelet coefficients for single-point uneven conditions at 100 different speeds: (a) measurement point 1; (b) measurement point 2; (c) measurement point 3; (d) measurement point 4.

The sum of wavelet coefficients for the multi-point irregularity condition is shown in Figure 12. The wavelet coefficients and the degree of abrupt variation of the multi-point non-smooth condition are significantly larger than those of the single-point non-smooth condition. In addition, the number of local peak points of the wavelet coefficients is also larger.

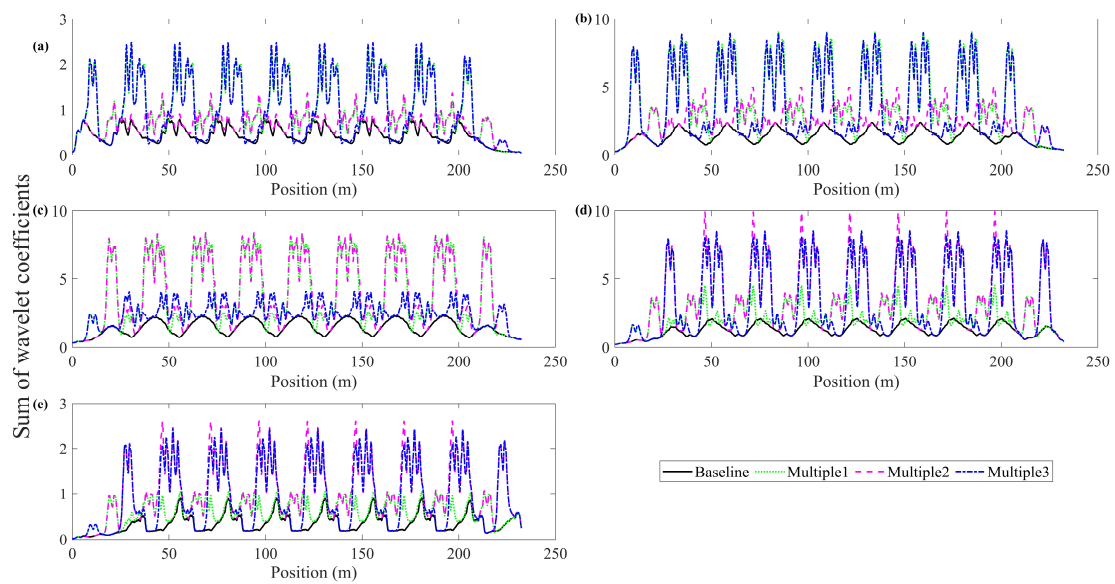


**Figure 12.** Sum of wavelet coefficients for multi-point uneven conditions at a speed of 200 km/h: (a) measurement point 1; (b) measurement point 2; (c) measurement point 3; (d) measurement point 4; (e) measurement point 5.

#### 4.4. Implementation Cases for Local Track Irregularity Localization

The example of two such conditions illustrate the localization process of the algorithm, single-1 and multiple-1, at a vehicle speed of 200 km/h. The wavelet coefficients sum curves of single-1 and multiple-1 compared with the baseline conditions are shown in Figures 13 and 14.

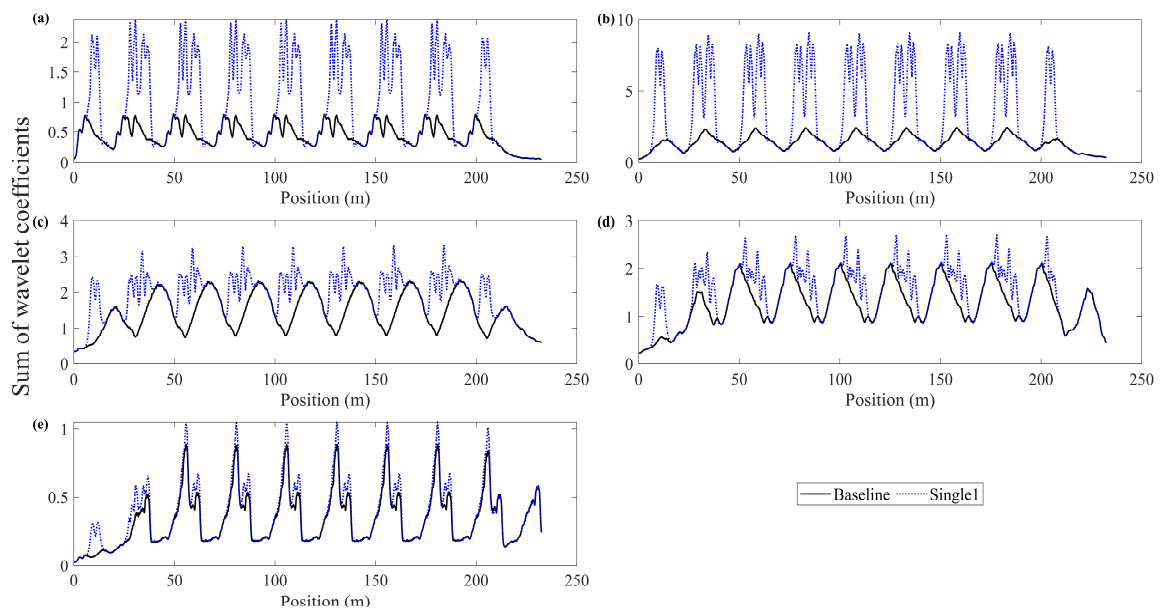


**Figure 13.** Comparison of sum of wavelet coefficients between single-1 and the baseline case: (a) measurement point 1; (b) measurement point 2; (c) measurement point 3; (d) measurement point 4; (e) measurement point 5.

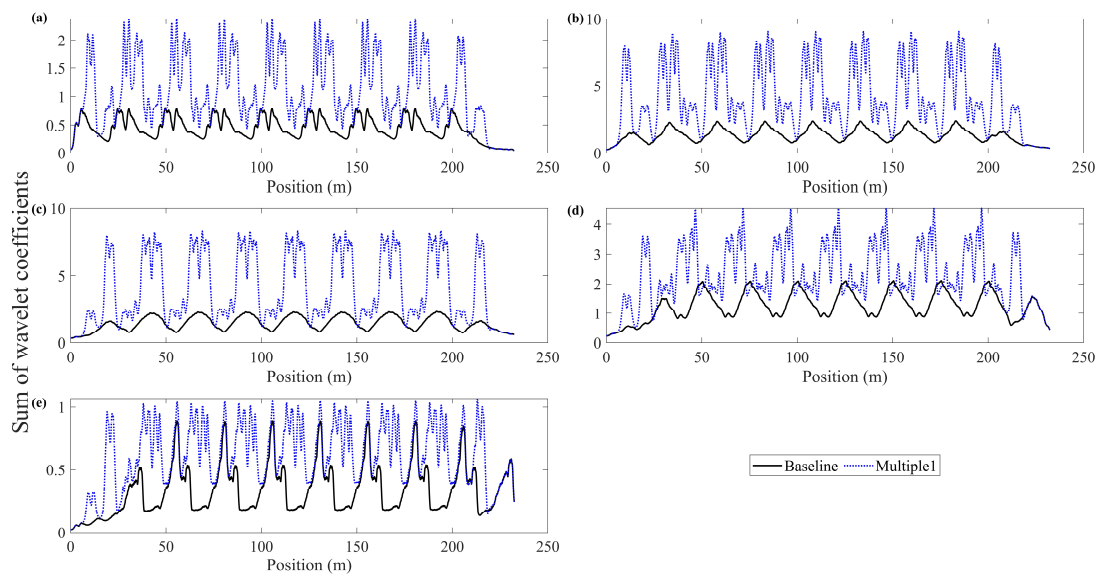


**Figure 14.** Comparison of sum of wavelet coefficients between multiple-1 and the baseline case: (a) measurement point 1; (b) measurement point 2; (c) measurement point 3; (d) measurement point 4; (e) measurement point 5.

As shown in Figure 13a,b, under the single-1 condition, the sum of wavelet coefficients of measuring point 1 and measuring point 2 has the largest mutation degree. It indicates that there is local irregularity near these two measuring points. Similarly, the multiple-1 condition was then analyzed. From Figure 13, it can be seen that the measuring points 1–3 are relatively close to the local irregularity. In summary, the sum of wavelet coefficients of measurement points 1–2 and 1–3 are selected for locating the local track irregularity of conditions single-1 and multiple-1, respectively.

The index-2, the local peak of the sum of the wavelet coefficients, is used for positioning. Figures 15 and 16 are the local peak points identified under single-1 and multiple-1 conditions, respectively. The first local peak identified by measuring points 1 and 2 is 9 m. The spatial interval of the remaining local peak points is consistent with the spatial distribution of the wheel. It shows that there is a local irregularity near 9m. The identification result is close to the local irregularity position of single point 1.

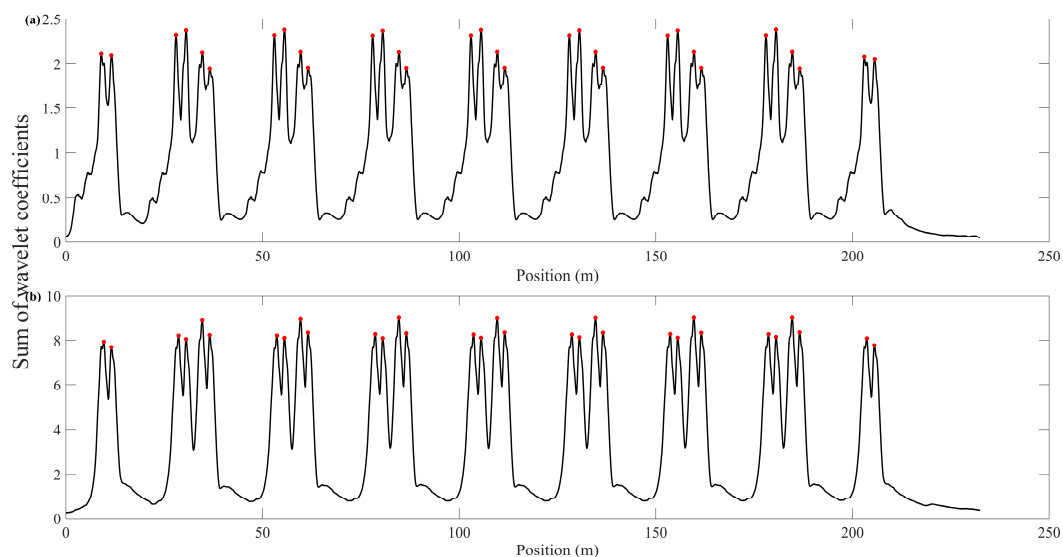


**Figure 15.** Local peaks of wavelet coefficient sum under single-1: (a) measurement point 1; (b) measurement point 2.

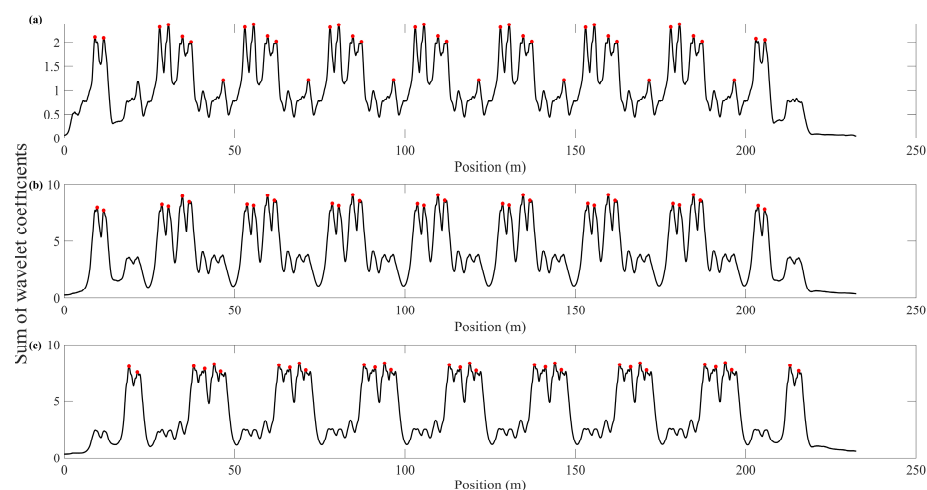


**Figure 16.** Local peaks of wavelet coefficient sum under multiple-1: (a) measurement point 1; (b) measurement point 2; (c) measurement point 3.

Similarly, the locations of the peak points shown in Figure 15 were analyzed. From this, it can be seen that measurement points 1 and 2 show a local irregularity near 9 m, and analysis of measurement point 3 shows a local irregularity near 19 m. The identification results indicate local irregularities at two locations in this case.

## 5. Conclusions

In this study, a local track irregularity identification method has been developed. The proposed approach utilizes CWT to extract multi-sensor time–frequency features of train-induced bridge accelerations. Since local irregularity will cause sudden changes in the time–frequency energy of bridge accelerations, the extracted features can be used to detect and locate local irregularity. A TTBI dynamic simulation was used to verify the feasibility and effectiveness of the algorithm. The effects of vehicle speed and location of local irregularity were investigated, through which main conclusions can be drawn as follows:

- The action of the local harmonic irregularity on the bridge structure can be equated to the action of the moving simple harmonic load. Local harmonic irregularities in the track structure will result in additional mid- and high-frequency components in the bridge acceleration response. Moreover, these additional frequency components are related to the train speed and the wavelength of the local harmonic irregularities.
- The sum of the wavelet coefficients in the full scale was used as the local track irregularity detection index-1, which reflects the change of the time–frequency energy of the bridge acceleration with the train running position. When the train passes through the location of local irregularity, the index will have a sudden change in the spatial domain. Moreover, the degree of mutation is related to the distance from the measuring point to local irregularity. When the measurement point is closer to the local irregularity position, the peak of index-1 mutation is greater and vice versa.
- The local peak points of index-1 are used as index-2 to locate local irregularity. As many carriages pass through local irregularity, the identified local peak points have relatively obvious periodic intervals in the spatial domain, which is related to the position of the wheels in the spatial domain. The two indexes proposed in this paper have relatively strong robustness to train speed and local irregularity position, and index-2 can identify multi-point local irregularity positions.

Future studies will study temperature and other environmental conditions and the effect of noise levels on the proposed method. The next step will be to adjust the process of the proposed method to reduce the influence of environmental factors on the identification

results. A possible issue to be addressed in the future is the effect of different baseline orbit upset spectra on the identification results.

**Author Contributions:** All authors participated in the discussions and made scientific contributions. Conceptualization, S.L.; Formal analysis, Y.Z.; Funding acquisition, S.L.; Investigation, Y.M.; Methodology, Y.M.; Project administration, S.L.; Software, Y.Z.; Supervision, S.L.; Writing—original draft, Y.M.; Writing—review & editing, S.L. All authors have read and agreed to the published version of the manuscript.

**Funding:** The research described in this paper was financially supported by China Railway Design Corporation R&D Program [2020YY340619, 2020YY240604], and Fundamental Research Funds for the Central Universities [FRFCU5710051018].

**Conflicts of Interest:** The authors declare no conflict of interest.

## References

- Cantero, D.; Basu, B. Railway infrastructure damage detection using wavelet transformed acceleration response of traversing vehicle. *Struct. Control Health Monit.* **2015**, *22*, 62–70. [[CrossRef](#)]
- Garg, V.K.; Dukkipati, R.V. Chapter 3-Description of the Railway Vehicle Models and Track Geometry. In *Dynamics of Railway Vehicle Systems*; Garg, V.K., Dukkipati, R.V., Eds.; Academic Press: Cambridge, MA, USA, 1984; pp. 58–102.
- Bocciolone, M.; Caprioli, A.; Cigada, A.; Collina, A. A measurement system for quick rail inspection and effective track maintenance strategy. *Mech. Syst. Signal Process.* **2007**, *21*, 1242–1254. [[CrossRef](#)]
- Moritaka, H.; Matsumoto, T. Track measurement by Kyushu Shinkansen cars in commercial service. In *Proceedings of the Computers in Railways XII: Computer System Design and Operation in Railways and other Transit Systems*; WIT Press: Ashurst, UK, 2010; p. 147.
- Insa, R.; Inarejos, J.; Salvador, P.; Baeza, L. On the filtering effects of the chord offset method for monitoring track geometry. *Proc. Inst. Mech. Eng. Part F J. Rail Rapid Transit* **2012**, *226*, 650–654. [[CrossRef](#)]
- Kouroussis, G.; Connolly, D.P.; Alexandrou, G.; Vogiatzis, K. The effect of railway local irregularities on ground vibration. *Transp. Res. Part D Transp. Environ.* **2015**, *39*, 17–30. [[CrossRef](#)]
- Caprioli, A.; Cigada, A.; Raveglia, D. Rail inspection in track maintenance: A benchmark between the wavelet approach and the more conventional Fourier analysis. *Mech. Syst. Signal Process.* **2007**, *21*, 631–652. [[CrossRef](#)]
- Ning, J.; Lin, J.; Zhang, B. Time–frequency processing of track irregularities in high-speed train. *Mech. Syst. Signal Process.* **2016**, *66*, 339–348. [[CrossRef](#)]
- Karis, T.; Berg, M.; Stichel, S.; Li, M.; Thomas, D.; Dirks, B. Correlation of track irregularities and vehicle responses based on measured data. *Veh. Syst. Dyn.* **2018**, *56*, 967–981. [[CrossRef](#)]
- Lee, J.S.; Choi, S.; Kim, S.S.; Park, C.; Kim, Y.G. A Mixed Filtering Approach for Track Condition Monitoring Using Accelerometers on the Axle Box and Bogie. *IEEE Trans. Instrum. Meas.* **2012**, *61*, 749–758. [[CrossRef](#)]
- An, B.Y.; Wang, P.; Xu, J.M.; Chen, R.; Cui, D.B. Observation and Simulation of Axle Box Acceleration in the Presence of Rail Weld in High-Speed Railway. *Appl. Sci.* **2017**, *7*, 1259. [[CrossRef](#)]
- Karis, T.; Berg, M.; Stichel, S. Analysing the correlation between vehicle responses and track irregularities using dynamic simulations and measurements. *Proc. Inst. Mech. Eng. Part F J. Rail Rapid Transit* **2020**, *234*, 170–182. [[CrossRef](#)]
- Molodova, M.; Li, Z.; Núñez, A.; Dollevoet, R. Validation of a finite element model for axle box acceleration at squats in the high frequency range. *Comput. Struct.* **2014**, *141*, 84–93. [[CrossRef](#)]
- Li, Z.; Molodova, M.; Zhao, X.; Dollevoet, R. Squat Treatment by Way of Minimum Action Based on Early Detection to Reduce Life Cycle Costs. *Mech. Syst. Signal Process.* **2010**, *1*, 305–311. [[CrossRef](#)]
- Molodova, M.; Li, Z.L.; Dollevoet, R. Axle box acceleration: Measurement and simulation for detection of short track defects. *WEAR* **2011**, *271*, 349–356. [[CrossRef](#)]
- Yuan, Z.; Zhu, S.; Chang, C.; Yuan, X.; Zhang, Q.; Zhai, W. An unsupervised method based on convolutional variational auto-encoder and anomaly detection algorithms for light rail squat localization. *Constr. Build. Mater.* **2021**, *313*, 125563. [[CrossRef](#)]
- Zhang, Y.; Xie, X.; Li, H.; Zhou, B. An Unsupervised Tunnel Damage Identification Method Based on Convolutional Variational Auto-Encoder and Wavelet Packet Analysis. *Sensors* **2022**, *22*, 2412. [[CrossRef](#)]
- Li, H.; Lan, C.M.; Ju, Y.; Li, D.S. Experimental and Numerical Study of the Fatigue Properties of Corroded Parallel Wire Cables. *J. Bridge Eng.* **2012**, *17*, 211–220. [[CrossRef](#)]
- Li, S.; Zhu, S.; Xu, Y.-L.; Chen, Z.-W.; Li, H. Long-term condition assessment of suspenders under traffic loads based on structural monitoring system: Application to the Tsing Ma Bridge. *Struct. Control Health Monit.* **2012**, *19*, 82–101. [[CrossRef](#)]
- Li, H.; Mao, C.-X.; Ou, J.-P. Experimental and theoretical study on two types of shape memory alloy devices. *Earthq. Eng. Struct. Dyn.* **2008**, *37*, 407–426. [[CrossRef](#)]
- Bao, Y.; Shi, Z.; Beck, J.L.; Li, H.; Hou, T.Y. Identification of time-varying cable tension forces based on adaptive sparse time-frequency analysis of cable vibrations. *Struct. Control Health Monit.* **2017**, *24*, e1889. [[CrossRef](#)]
- Huang, Y.; Beck, J.L.; Li, H. Bayesian system identification based on hierarchical sparse Bayesian learning and Gibbs sampling with application to structural damage assessment. *Comput. Methods Appl. Mech. Eng.* **2017**, *318*, 382–411. [[CrossRef](#)]

23. Li, S.; Wei, S.; Bao, Y.; Li, H. Condition assessment of cables by pattern recognition of vehicle-induced cable tension ratio. *Eng. Struct.* **2018**, *155*, 1–15. [[CrossRef](#)]
24. Zhai, W.M.; Han, Z.L.; Chen, Z.W.; Ling, L.; Zhu, S.Y. Train-track-bridge dynamic interaction: A state-of-the-art review. *Veh. Syst. Dyn.* **2019**, *57*, 984–1027. [[CrossRef](#)]
25. Zhu, Z.H.; Gong, W.; Wang, L.D.; Bai, Y.; Yu, Z.W.; Zhang, L. Efficient assessment of 3D train-track-bridge interaction combining multi-time-step method and moving track technique. *Eng. Struct.* **2019**, *183*, 290–302. [[CrossRef](#)]
26. Yu, Z.W.; Mao, J.F. Probability analysis of train-track-bridge interactions using a random wheel/rail contact model. *Eng. Struct.* **2017**, *144*, 120–138. [[CrossRef](#)]
27. Xu, L.; Zhai, W.M.; Li, Z.L. A coupled model for train-track-bridge stochastic analysis with consideration of spatial variation and temporal evolution. *Appl. Math. Model.* **2018**, *63*, 709–731. [[CrossRef](#)]
28. Clough, R.W.; Penzien, J.; Griffin, D.S. *Dynamics of Structures*; McGraw Hill Inc.: New York, NY, USA, 1975.
29. Råde, L.; Westergren, B. *Mathematics Handbook for Science and Engineering*; Springer: Berlin/Heidelberg, Germany, 2010.
30. Wang, X.; Li, Z.; Zhuo, Y.; Di, H.; Wei, J.; Li, Y.; Li, S. Indirect displacement monitoring of high-speed railway box girders consider bending and torsion coupling effects. *Smart Struct. Syst.* **2021**, *28*, 827–838.

**Disclaimer/Publisher's Note:** The statements, opinions and data contained in all publications are solely those of the individual author(s) and contributor(s) and not of MDPI and/or the editor(s). MDPI and/or the editor(s) disclaim responsibility for any injury to people or property resulting from any ideas, methods, instructions or products referred to in the content.